The Formation of Mesoporous TiO_2 Spheres via a Facile Chemical Process

Yunxia Zhang,*,†,‡ Guanghai Li,† Yucheng Wu,‡ Yuanyuan Luo,† and Lide Zhang†

Key Laboratory of Materials Physics, Institute of Solid State Physics, Chinese Academy of Sciences, P.O. Box 1129, Hefei 230031, People's Republic of China and Department of Material Science and Engineering, Hefei University of Technology, Hefei 230009, People's Republic of China

Received: September 24, 2004; In Final Form: November 8, 2004

The mesoporous TiO_2 solid and hollow spheres have been synthesized via a controllable and simple chemical route. Structural characterization indicates that these TiO_2 mesoporous spheres after calcined at 500 °C have an obvious mesoporous structure with the diameters of 200−300 nm for solid spheres and 200−500 nm for hollow spheres. The average pore sizes and BET surface areas of the mesoporous TiO_2 solid and hollow spheres are 6.8, 7.0 nm and 162, 90 m^2/g, respectively. Optical adsorption investigation shows that TiO_2 solid and hollow spheres possess a direct band gap structure with the optical band gap of 3.68 and 3.75 eV, respectively. A possible formation mechanism for TiO_2 solid and hollow spheres is discussed.

Introduction

Since the M41S family of the ordered mesoporous silica was reported by Mobil,[1] mesoporous materials have attracted particular attention for adsorption, catalysis, and applications as hosts for nanomaterials synthesis as they usually show higher surface area and tunable pore structures compared with nanocrystalline materials;[2] in most cases, they display unique electronic, magnetic, and catalytic properties.[3] However, there have been few reports about mesoporous transition-metal oxides. Among the transition-metal oxides, TiO_2 has been widely used as chemical sensing, catalysis, energy conversion, sorption media, filters, and photocatalysis.[4] Mesoporous structure TiO_2 should be an even more effective catalyst because of its large surface area and porous frameworks.[5−9] Recently, Zhang et al. found that TiO_2 microspheres with porous structures have higher photocatalytic activity and are easy to be recovered and used repeatedly.[10] The breakthrough will open a novel pathway for the elevation of the photocatalysis of TiO_2 materials.

Mesoporous TiO_2 was first synthesized through modified sol−gel routes in the presence of alklyphosphate surfactant templates by Antonelli and Ying in 1995.[11] After that, many different routes about the synthesis of mesoporous TiO_2 spheres have been reported constantly. Yang et al. reported the synthesis of anatase TiO_2 nanospheres via Ostwald ripening after a longer hydrothermal treatment.[12] Dong et al. prepared mesoporous spheres of metal oxides on the basis of the two-step nanocasting route.[13] Recently, Ren et al. have prepared hollow microspheres of mesoporous TiO_2 adopting the surfactant-assisted method.[14] However, up to now, most of the syntheses of mesoporous TiO_2 use unavoidly ionic liquid,[15] block polymer,[16] surfactants,[14] and so forth as the structure-directing template. It is still a great challenge to develop a new free template and mass-production available route to synthesize mesoporous TiO_2 spheres.

In this paper, we describe a facile chemical process to synthesize mesoporous TiO_2 submicrometer spheres and realize the control of solid or hollow spheres by simply adjusting the adding order of the reactants, which do not need the use of surfactants or other templates. These mesoporous TiO_2 solid spheres themselves will be better catalytic carriers. The mesoporous TiO_2 hollow spheres will open up various new applications such as controlled release capsules, artificial cells or drug delivery, lightweight structural materials, shape-selective adsorbents, and catalysts.

Experimental Section

Samples Preparation. In a typical preparation process of mesoporous TiO_2 solid spheres, 6 mL of titanium butoxide was dissolved in 40 mL absolute ethanol. Then, 0.0015 mol citric acid, 2 mL distilled water, and 20 mL concentrated $NH_3 \cdot H_2O$ were added to the above solution in turn. After sufficiently stirring for several hours, the mixed solution was left to stand for overnight. Then, the white precipitate was filtered, washed with distilled water and ethanol, and dried at 60 °C for 8 h. Finally, the powder was calcined at 500 °C for 4 h. As for the mesoporous TiO_2 hollow spheres, 0.0015 mol citric acid was first dissolved in the solution of 40 mL absolute ethanol and 2 mL distilled water, then 10 mL of concentrated $NH_3 \cdot H_2O$ was added to the resulting solution, leading to the formation and growth of ammonium citrate crystals. Finally, 6 mL of titanium butoxide and 10 mL of ammonium were dipped in the above solution simultaneously. The dipping rate for ammonia is about 2 times that for titanium butoxide. The subsequent processes are the same as that for TiO_2 solid spheres.

Characterization. The purity and composition of the products were characterized by powder X-ray diffraction (XRD) using a Rigaku D/Max γA X-ray diffractometer with Cu Kα radiation ($\lambda = 1.54178$ Å). The morphologies were observed with a field emission scanning electron microscope (FESEM) and a transmission electron microscope (TEM, Hitachi H-800). The nitrogen adsorption−desorption isotherm was measured on an Omnisorp 100CX. Infrared spectra were measured on the Fourier infrared spectrum instrument (Nicolet Magna-IR750). Absorption spectrum was measured on a UV−vis spectrophotometer (Shimadzu UV-240) in the wavelength range of 200−800 nm.

* To whom correspondence should be addressed. E-mail: zyxqm@yahoo.com.cn.
† Institute of Solid State Physics, Chinese Academy of Sciences.
‡ Hefei University of Technology.

10.1021/jp0456640 CCC: $30.25
Published on Web 03/05/2005

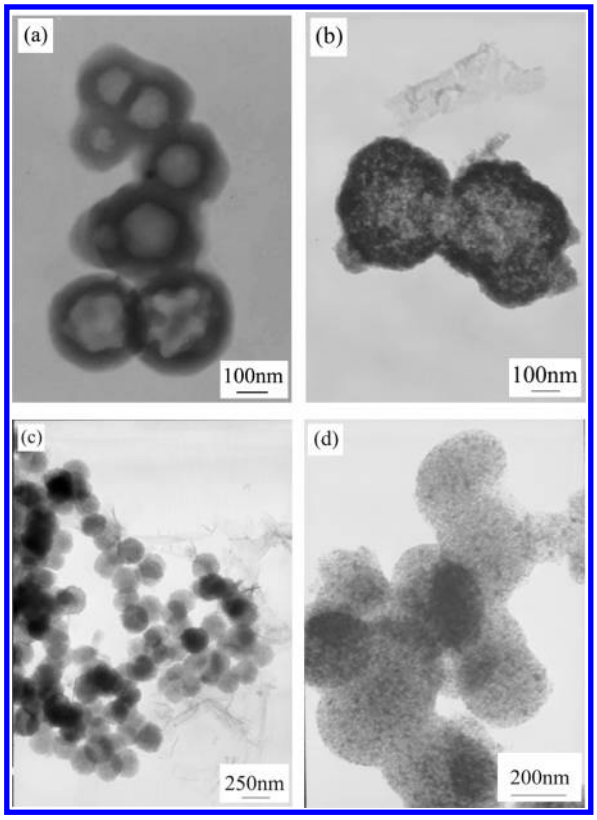

Figure 1. TEM images of mesoporous TiO_2 spheres before ((a): hollow; (c): solid) and after calcination ((b): hollow; (d): solid).

Results and Discussion

FESEM analyses were performed to examine the morphology of TiO_2 spheres. Figure S1 represents FESEM images of TiO_2 solid and hollow spheres. The TiO_2 spheres are 200−300 nm in diameter for solid spheres and 200−500 nm for hollow spheres. The inset in Figure S1b shows a few broken hollow spheres. The partly fractured spherical particles show that these spheres are hollow inside. Although the proportion of broken spheres appears to be smaller from SEM observation, the actual proportion could be somewhat larger than that of observation as there may be some broken spheres with their holes upside down. In addition, it is possible that the hollow spheres are very hard to break because of excellent tenacity, which makes it difficult to observe the hollow spheres. TEM observations further display the morphologies of these spheres. Figure 1a and b shows two TEM images of the mesoporous TiO_2 hollow spheres before and after calcined at 500 °C, respectively. Figure 1 c and d is that of the mesoporous TiO_2 solid spheres before and after calcination at 500 °C, respectively. Apparently, each sphere after calcination is composed of a large amount of very small particles with the average size of about 7 nm and constitutes a disordered wormhole framework, which is a typical characteristic of mesoporous structures, and this mesoporous structure could not be observed before calcination. TiO_2 microspheres are very stable and the mesoporous structure did not collapse after calcination at 500 °C for 4 h. TiO_2 spheres either solid or hollow are of amorphous structure after directly drying at 60 °C and are of anatase structure after calcination at 500 °C for 4 h, which can be characterized by X-ray diffraction (XRD) patterns (Figure S2). According to the Scherrer equation, the average crystalline size of TiO_2 spheres after calcination is all about 7 nm, which is basically in agreement with the results of TEM.

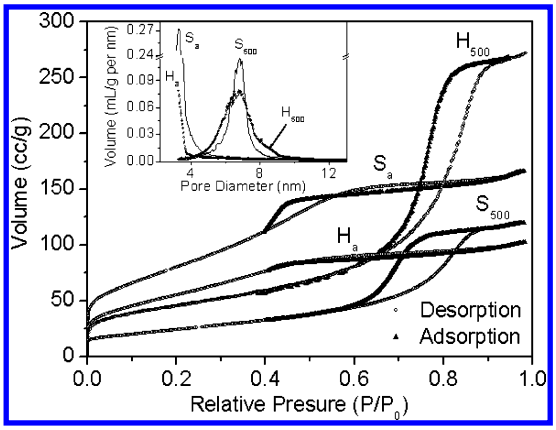

Figure 2. Nitrogen adsorption−desorption isotherm and pore size distribution (in the inset) of mesoporous TiO_2 spheres (H: hollow; S: solid; subscript a: before calcination; subscript 500: after calcined at 500 °C for 4 h).

The surface area and porosity of the TiO_2 microspheres are investigated using the nitrogen adsorption and desorption isotherm (shown in Figure 2). It can be seen from this figure that there is no pore for the TiO_2 hollow spheres before calcination, and there is a very small amount of pore with an average pore diameter ca. 3.5 nm for the TiO_2 solid spheres before calcination. After calcination at 500 °C for 4 h, both isotherms are of a typical IV-like isotherm with a type H_2 hysteretic loop, indicating the presence of mesoporous materials according to the IUPAC classification.[17] The plots of the pore size distribution (inset in Figure 2) are determined by the BJH (Barrett−Joyner−Halenda) method from the desorption branch of the isotherm, which shows that these TiO_2 microspheres after calcination have very obvious mesoporous structure. The average pore diameters of TiO_2 hollow and solid spheres after calcination are 6.8 and 7.0 nm, respectively. In addition, the mesopore size distribution for TiO_2 solid spheres is narrower than that for TiO_2 hollow spheres according to the inset in the Figure 2. The narrower size distribution indicates better homogeneity of the pores for the solid spheres. The BET surface areas of TiO_2 hollow and solid spheres before calcination are about 202 and 290 m^2/g, respectively, and these values decrease to about 90 and 162 m^2/g, respectively, because of the crystallization and increase in the size of TiO_2 particles. The relative low BET surface area for TiO_2 hollow spheres might be due to its broad size distribution.

The band gap of semiconductor nanomaterials will increase with the decrease of particle size, which leads to the move of the absorption edge to a high energy; this is the so-called quantum size effect. The optical band gaps of the calcined mesoporous TiO_2 spheres are studied by UV−vis optical absorbance spectra. The optical band gap energy, E_g, is determined from the absorption spectra, where a steep increase of the absorption is observed because of a band−band transition, from the general relation[18]

$$(\alpha h\nu)^n = B(E - E_g)$$

where B is the constant related to the effective masses associated with the valence and conduction bands, E_g is the band gap energy, $E = h\nu$ is the photon energy, and $n = 1/2$ or 2, depending on whether the transition is indirect or direct, respectively.

Figure 3 shows the absorption spectra of the mesoporous TiO_2 spheres after calcination. The inset shows the plots of $(\alpha h\nu)^2$ verses the photo energy ($h\nu$). The band gap energy (E_g) for the

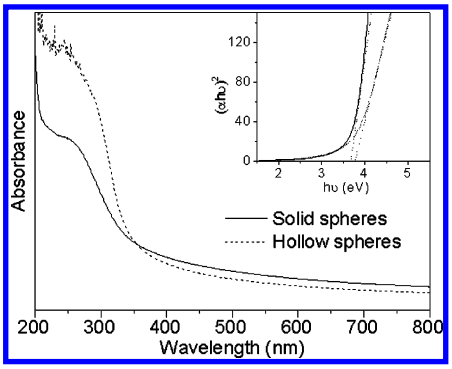

Figure 3. Absorbance spectra of the mesoporous TiO_2 solid and hollow spheres after calcination. The inset is a plot of $(\alpha h\nu)^2$ vs $h\nu$.

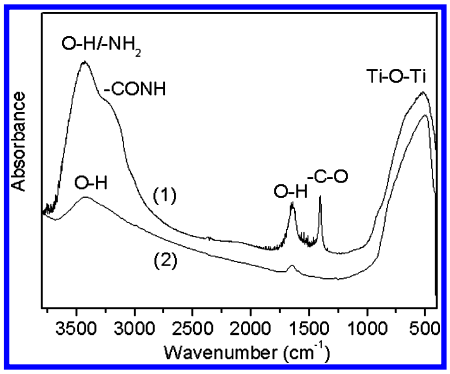

Figure 4. FTIR spectra of the mesoporous TiO_2 solid spheres before (curve 1) and after (curve 2) calcination.

mesoporous TiO_2 spheres can be calculated by extrapolating the linear portion of $(\alpha h\nu)^2$ versus $h\nu$ plot to $\alpha = 0$. On the basis of these, the optical band gaps for the TiO_2 hollow spheres and solid spheres are of 3.75 and 3.68 eV, respectively, which are all higher than that of anatase TiO_2 nanoparticles with the particle size of 5−10 nm (3.36 eV).[19] This obvious blue shift of the optical band gap might be due to both the smaller average crystal size and a relative uniform crystal size distribution of the mesoporous TiO_2 spheres. The best fit of the optical band gap using $n = 2$ indicates that the direct transition for the mesoporous TiO_2 spheres is the dominant transition involved.

The FTIR spectra of the mesoporous TiO_2 solid spheres are shown in Figure 4. Before calcination, there are some absorbances at 3428, 3223, 1644, and 1400 cm^{-1} originated from the vibrations of −OH, −CONH, −OH, and −C−O. After calcination, the absorbance peaks at 3223 and 1400 cm^{-1} due to carboxylate group disappeared. The absorbances between 500 and 900 cm^{-1} originated from the titanium dioxide. The presence of water is supported by the appearance of the bending mode at 1640 cm^{-1} and the stretching mode at 3400 cm^{-1}. The same results are also obtained for the mesoporous TiO_2 hollow spheres. The result indicates that the ammonium citrate appears in the mesoporous TiO_2 spheres before calcination and disappears after calcination at 500 °C for 4 h; the existence of ammonium citrate crystals within mesoporous TiO_2 spheres even after washing-up by distilled water and ethanol further proved that the ammonium citrate crystals are wrapped by TiO_2 nanoparticles. It also can be seen that the OH bending and stretching mode exists before calcination; this surface hydroxylation is very advantageous for the photocatalytic activity of anatase because it provides higher capacity for oxygen adsorption.[20, 21]

Although the exact formation mechanism of the mesoporous TiO_2 spheres is not very clear, we think that the ammonium citrate might play a key role in the formation of the mesoporous spheres since only TiO_2 nanoparticles were obtained without citric acid. To examine the existence of ammonium citrate crystals, a contrast experiment was performed adopting a similar process for the preparation of mesoporous TiO_2 hollow spheres without titanium butoxide. SEM (in Figure S3) shows the presence of a large amount of ammonium citrate crystals with short rods or particles shape, which provides some proof for the formation of the hollow structure of TiO_2 spheres. Indeed, the ammonium citrate crystals emerged in the TiO_2 solid spheres should be smaller than those observed in SEM because of the confined effect of TiO_2 sols. Also, the growth kinetics is very important for the formation of the mesoporous spheres. The formation of mesoporous TiO_2 solid or hollow spheres was highly dependent on the extent of TiO_2 condensation present at the onset of ammonium citrate crystals growth. That is, mesoporous solid spheres were formed when TiO_2 condensation process takes place with the formation of ammonium citrate crystals simultaneously; mesoporous hollow spheres were produced when the nucleation and growth of ammonium citrate crystals happen before the TiO_2 condensation process.

SCHEME 1: Schematic Illustration of the Formation Mechanisms for the Mesoporous TiO_2 Hollow and Solid Spheres

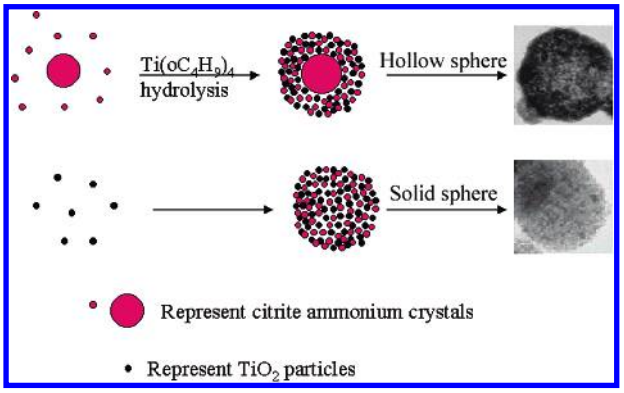

Scheme 1 is a simple model of the formation mechanism of the mesoporous TiO_2 hollow and solid spheres. When ammonia was first added to the mixture of water, alcohol, and citrate acid, the ammonium citrate solution formed at the beginning reaction. The ammonium citrate will be in supersaturation state with the dripping of ammonia, which will lead to the separation and growing up of these ammonium citrate crystals via Ostald ripening mechanism. The size and content of ammonium citrate crystals depend on the dipping speed and content of ammonia. These larger ammonium citrate crystals are serving as the nucleation centers of TiO_2 spheres. Since titanium butoxide and the residual ammonia were simultaneously dipped, the following ammonium citrate crystals have no chance to grow up. These smaller ammonium citrate crystals are nucleation centers of TiO_2 particles in spherical walls. In this way, the mesoporous TiO_2 hollow spheres are formed through subsequent washing and calcination. However, when distilled water and ammonia are dipped into the alcohol solution composed of titanium and citric acid, the ammonium citrate crystals will be surrounded immediately by TiO_2 colloid particles before they have enough time to grow up, which will lead to the formation of the mesoporous TiO_2 solid spheres.

Conclusion

In conclusion, we successfully realized the controlled synthesis of the mesoporous TiO_2 solid and hollow spheres via a facile chemical process. This method is very simple and easy

to scale-up and might be extended to the preparation of the hollow microspheres of other inorganic oxides. Furthermore, the optical band gap of these mesoporous TiO_2 spheres has obvious blue shift compared with anatase TiO_2 nanoparticles with the similar size. The mesoporous TiO_2 sphere is a better candidate for applications in catalysis, biomaterials, microelectronics, optoelectronics, and photonics.

Acknowledgment. This work was supported by National Major Project of Fundamental Research: Nanomaterials and Nanostructures (Grant No. G19990645).

Supporting Information Available: FESEM images of the mesoporous TiO_2 solid and hollow spheres, X-ray diffraction pattern of the mesoporous TiO_2 spheres before and after calcination, and SEM image of ammonium citrate crystals formed without titanium butoxide. This material is available free of charge via the Internet at http://pubs.acs.org.

References and Notes

(1) Kresge, C. T.; Leonowicz, M. E.; Roth, W. J.; Vartuli, J. C.; Breck, J. S. *Nature* **1992**, *359*, 710.
(2) Yada, M.; Ohya, M.; Machida, M.; Kijima, T. *Langmuir* **2000**, *16*, 4752.
(3) Hwang, Y. K.; Lee, K. C.; Kwon, Y. U. *Chem. Commun* **2001**, 1738.
(4) Hagfeldt, A.; Grätzel, M. *Chem. Rev.* **1995**, *95*, 49.
(5) Wang, Y.; Tang, X.; Yin, L.; Huang, W.; Hacohen, Y. R.; Gedanken, A. *Adv. Mater.* **2000**, *12*, 1183.
(6) Yu, J. C.; Zhang, L.; Yu, J. *Chem. Mater.* **2002**, *14*, 4647.
(7) Luo, H.; Wang, C.; Yan, Y. *Chem. Mater.* **2003**, *15*, 3841.
(8) Yun, H.; Miyazawa, K.; Zhou, H.; Honma, I.; Kuwabara, M. *Adv. Mater.* **2001**, *13*, 1377.
(9) Kluson, P.; Kacer, P.; Cajthaml, T.; Kalaji, M. *J. Mater. Chem.* **2001**, *11*, 644.
(10) Zhang, B. L.; Chen, B. S.; Shi, K. Y.; He, S. J.; Liu, X. D.; Du, Z. J.; Yang, K. L. *Appl. Catal., B: Environ.* **2003**, *40*, 253.
(11) Antonelli, D. M.; Ying, Y. J. *Angew. Chem., Int. Ed. Engl.* **1995**, *34*, 2014.
(12) Yang, H. G.; Zeng, H. C. *J. Phys. Chem. B* **2004**, *108*, 3492.
(13) Dong, A. G.; Ren, N.; Tang, Y.; Wang, Y. J.; Zhang, Y. H.; Hua, W. M.; Gao, Z. *J. Am. Chem. Soc.* **2003**, *125*, 4976.
(14) Ren, T.-Z.; Yuan, Z.-Y.; Su, B.-L. *Chem. Phys. Lett.* **2003**, *374*, 170.
(15) Zhou, Y.; Antonietti, M. *J. Am. Chem. Soc.* **2003**, *125*, 14960.
(16) Yue, Y. H.; Gao, Z. *Chem. Commun.* **2000**, 1755.
(17) Sing, K. S. W. *Pure Appl. Chem.* **1982**, *54*, 2201.
(18) Van Leeuwen, R. A.; Hung, C.-J.; Kammler, D. R.; Switzer, J. A. *J. Phys. Chem.* **1995**, *99*, 15247.
(19) Reddy, K. M.; Manorama, S. V.; Reddy, A. R. *Mater. Chem. Phys.* **2002**, *78*, 239.
(20) Ohtani, B.; Ogawa, Y.; Nishimoto, S. *J. Phys. Chem.* **1997**, *101*, 3746.
(21) Anderson, C.; Bard, A. J. *J. Phys. Chem.* **1995**, *99*, 9882.